

Background-free quantum frequency conversion of single photons from a semiconductor quantum dot

Serkan Ates,^{1,2,*} Imad Agha,^{1,2} Antonio Badolato,³ and Kartik Srinivasan^{1,†}

¹*Center for Nanoscale Science and Technology, National Institute of Standards and Technology, Gaithersburg, MD 20899, USA*

²*Maryland NanoCenter, University of Maryland, College Park, MD*

³*Department of Physics and Astronomy, University of Rochester, Rochester, New York 14627, USA*

(Dated: June 20, 2018)

We demonstrate background-free quantum frequency conversion of single photons from an epitaxially-grown InAs quantum dot. Single photons at ≈ 980 nm are combined with a pump laser near 1550 nm inside a periodically-poled lithium niobate (PPLN) waveguide, generating single photons at ≈ 600 nm. The large red-detuning between the pump and signal wavelengths ensures nearly background-free conversion, avoiding processes such as upconversion of anti-Stokes Raman scattered pump photons in the PPLN crystal. Second-order correlation measurements on the single photon stream are performed both before and after conversion, confirming the preservation of photon statistics during the frequency conversion process.

Quantum frequency conversion [1] is a useful resource in interfacing quantum systems that can be connected by photons but which operate at disparate frequencies. It has been enabled by the development of high-efficiency frequency conversion techniques in $\chi^{(2)}$ [2] and $\chi^{(3)}$ materials [3, 4], and been demonstrated in experiments in which the quantum state of a light field was shown to be preserved during the process [5–11]. Other experiments have focused on the benefits associated with shifting the frequency of light to a wavelength band in which high-efficiency detectors exist [12–16]. Ideally, quantum frequency conversion should be background-free and avoid the generation of noise photons that are spectrally unresolvable from the frequency-converted quantum state. Sum- and difference-frequency generation in $\chi^{(2)}$ materials [1] and four-wave-mixing Bragg scattering in $\chi^{(3)}$ materials [17] can be, in principle, background-free, meaning that signal photons are directly converted to idler photons without amplification of vacuum fluctuations, which can occur in processes such as degenerate four-wave-mixing [17]. However, other processes, such as broadband Raman scattering of pump photons, may still be a source of noise. Indeed, frequency conversion of Raman noise photons is a major noise source in $\chi^{(2)}$ systems such as quasi-phase-matched periodically-poled lithium niobate (PPLN) waveguides [13], and was the dominant noise source in a recent demonstration of frequency conversion of single photon Fock states [8], limiting the purity of the frequency-converted single photon source.

Here, we demonstrate nearly background-free quantum frequency conversion of single photons from a semiconductor quantum dot. We work with quantum dots emitting in the well-studied 900 nm to 1000 nm wavelength range [18–21], and convert their single photon emission to 600 nm. By using a much wider wavelength separation between the signal and pump photons, we show that the signal-to-background level improves by about two orders of magnitude with respect to Ref. 8. Measurements of the photon statistics before and after conversion indicate

essentially no degradation in purity of the single photon stream due to the frequency conversion process.

The experimental system we use for quantum frequency conversion experiments is depicted in Fig. 1(a). Our source of single photons is a single InAs quantum dot (QD) in a fiber-coupled, GaAs microdisk optical cavity [22], which is excited above the GaAs band-edge by a continuous wave (cw) or pulsed (50 MHz repetition rate, 50 ps pulse width) 780 nm fiber-coupled laser diode. While our previous work [8] was focused on telecommunications-band (1300 nm) to visible band (710 nm) wavelength conversion, here our QD emits photons at ≈ 980 nm. Emission from the QD is out-coupled by a fiber taper waveguide (FTW) and spectrally isolated using a ≈ 0.2 nm bandwidth volume reflective Bragg grating whose input and output is coupled to single mode optical fiber. At this point, we can either perform photon correlation measurements on the 980 nm signal using a standard Hanbury-Brown and Twiss (HBT) setup [18], or send it to the frequency conversion setup. In the frequency conversion setup, we use a wavelength division multiplexer (WDM) to combine the spectrally-filtered QD emission with a strong (few hundred mW) 1550 nm pump signal that is generated by an external cavity tunable diode laser and erbium-doped fiber amplifier (EDFA). Fiber polarization controllers (FPCs) are used to adjust the polarization state of both the 980 nm and 1550 nm beams. The combined signal and pump are coupled into a 2 cm long, 5 % MgO-doped PPLN waveguide whose temperature can be adjusted between 25 °C and 90 °C with 0.1 °C resolution. Light is coupled into the waveguide through a cleaved single mode optical fiber that is controlled by a 3-axis open-loop piezo stage and has a mode-field diameter of 5.8 μm at 980 nm. The coupling is optimized for the 980 nm band signal, at the expense of the 1550 nm pump (additional pump power compensates for the 1550 nm coupling inefficiency). Light exiting the PPLN waveguide is collimated and sent through two dispersive prisms and two 750 nm short pass edge fil-

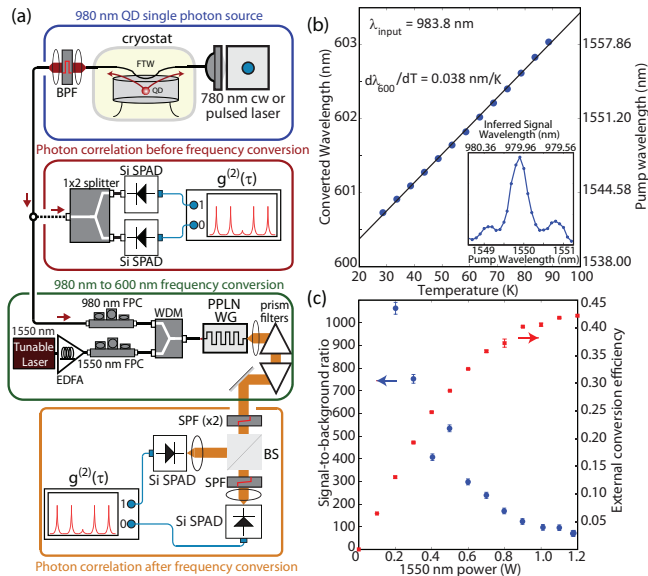


FIG. 1. (a) Schematic of the experimental setups used within this work. (b) Plot of the 600 nm band wavelength as a function of PPLN waveguide temperature, for a fixed 983.8 nm signal and 1550 nm pump wavelength adjusted to maximize the converted signal. The inset shows the quasi-phase-matching response of the PPLN waveguide, with the signal fixed at 980 nm and 1550 nm pump wavelength varied. (c) Signal-to-background ratio (left y-axis, blue points) and external conversion efficiency (right y-axis, red points) as a function of 1550 nm pump power coupled into the 980 nm/1550 nm WDM. The external conversion efficiency includes all losses in the system. The overall detection efficiency of the frequency conversion system is given as the product of the external conversion efficiency and the detector quantum efficiency ($\approx 67\%$) [23].

ters (SPFs) to eliminate residual 1550 nm pump photons and frequency doubled 775 nm pump photons from the signal. A second HBT setup is used to measure photon statistics of the frequency converted signal.

We assess the properties of the frequency conversion setup by using a narrow (<5 MHz) linewidth 980 nm band laser attenuated to a power level of ≈ 30 fW, similar to the expected average power levels of our QD single photon sources. First, we measure the quasi-phase-matching bandwidth of the PPLN waveguide. The temperature of the PPLN waveguide is set to 58.8 °C, and the 1550 nm pump power is set to ≈ 800 mW, close to the value at which we achieve optimal conversion efficiency (described further below). We then scan the 1550 nm pump wavelength while monitoring the frequency converted 600 nm band signal on a silicon single-photon avalanche diode (SPAD), as shown in the inset to Fig. 1(b). The curve approximately follows the theoretically expected sinc^2 response [2], and the inferred bandwidth in the 980 nm band (determined by energy conservation) is ≈ 0.20 nm. We next repeat this measurement while keeping the signal wavelength fixed at 983.8 nm and

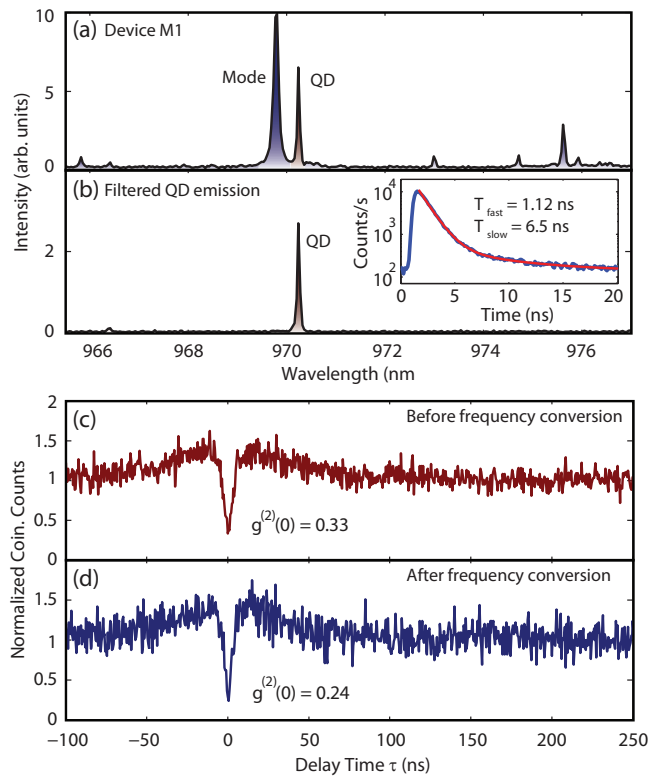


FIG. 2. (a) Low-temperature μ -PL spectrum of device M1 under above-band cw excitation ($\lambda_{exc.} = 780$ nm), showing a single QD emission and a nearby cavity mode ($Q = 12500$) around 970 nm. (b) Spectrum of QD emission filtered by a volume Bragg grating. (c)-(d) Second-order autocorrelation function measurements performed on the QD emission line before and after the frequency conversion resulted in $g^{(2)}(0) = 0.33 \pm 0.03$ and $g^{(2)}(0) = 0.24 \pm 0.04$, respectively. inset: Time-resolved PL of the QD emission revealed $T_{fast} = 1.12$ ns ± 0.05 ns and $T_{slow} = 6.5$ ns ± 0.1 ns.

varying the PPLN waveguide temperature. The resulting plot of frequency converted wavelength in the 600 nm band against PPLN waveguide temperature is shown in Fig. 1(b), and indicates that the output emission can be tuned by ≈ 2 nm. This tuning would be needed for precise spectral matching of the frequency-converted single photons with a resonant quantum system operating near 600 nm. We also perform experiments in which the 980 nm signal wavelength is varied, and the PPLN waveguide temperature and 1550 nm band pump wavelength are adjusted to achieve phase-matching. We observe that we can efficiently ($> 35\%$ external conversion efficiency) convert signals in the wavelength region between 970 nm and > 995 nm (the upper wavelength limit of our laser), covering nearly the entire s-shell emission range of the QD ensemble. This means that QDs emitting at different wavelengths (unavoidable due to size dispersion during growth) can be frequency converted to the same wavelength.

In our previous work [8], in which the signal was

at 1300nm and pump at 1550nm, frequency conversion of anti-Stokes photons generated by Raman scattering of the 1550nm pump was thought to be the dominant source of noise, limiting the achievable signal-to-background levels to about 7:1 (and as low as 2:1 for the highest conversion efficiencies). Use of a pulsed pump at 1550 nm [24] removes background emission that is temporally distinguishable from the single photon emission, but does not improve the signal-to-background level. While better spectral filtering does improve this ($> 10:1$ signal-to-background levels were reported in a recent single photon downconversion experiment [11]), it is perhaps more desirable to suppress the source of the noise, for example, by increasing the separation between the signal and red-detuned pump [13, 25, 26]. Here, our pump-signal separation is nearly 600nm, suggesting that the signal-to-background levels might be significantly improved. To test this, we measure (Fig. 1(c)) the signal-to-background level as a function of 1550nm band pump power, determined by comparing the ratio of the detected counts on the SPAD with and without the presence of the 980nm band signal (and after subtraction of the SPAD dark count rate of $\approx 50 \text{ s}^{-1}$). On the same graph, we plot the external conversion efficiency of the system, which includes all PPLN waveguide input/output coupling, free-space transmission, and spectral filtering losses (detector quantum efficiency is not included). At the lowest 1550nm pump powers (measured at the input of the 980nm/1550nm WDM), for which the conversion efficiency is just a few percent, the signal-to-background level exceeds 1000. As the pump power increases, the signal-to-background level decreases, but still remains above 100 for all but the highest 1550nm pump powers, where the conversion efficiency has begun to roll off. For the experiments that follow, we operate with a 35 % to 40 % external conversion efficiency, slightly higher than that used in ref. 8, and a signal-to-background level > 100 , exceeding that used in our previous work by nearly two orders of magnitude. As the PPLN incoupling efficiency is $\approx 60 \%$, and the transmission through all optics after the PPLN waveguide is $\approx 80 \%$, the internal conversion efficiency in the PPLN waveguide is $> 70 \%$.

As mentioned above, single InAs QDs embedded in microdisk cavities are used as true single photon sources for the quantum frequency conversion experiments. Here, we present results from two microdisk devices named as M1 and M2. Figure 2(a) shows a low temperature ($T = 10 \text{ K}$) micro-photoluminescence ($\mu\text{-PL}$) spectrum of device M1, which was obtained under cw excitation with an energy above the GaAs bandgap. Two bright lines seen in the spectrum are identified as a neutral excitonic emission from a single QD (970.2nm) and a cavity mode emission (969.8nm) with a quality factor $Q = 12500$. The identification of the lines is done based on their excitation power dependence, which revealed first a linear increase with the power and then a clear saturation for the QD

line, while the cavity mode emission dominated the spectrum at elevated power conditions as expected. For further investigations, the QD emission line was spectrally filtered by using a volume Bragg grating whose output was coupled to a single mode fiber. Figure 2(b) shows the filtered spectrum of the QD emission with almost 60 % total transmission. The filtered PL spectrum was first directed to a time-correlated single-photon counting setup for time-resolved PL measurements. The lifetime [27] of the emission is estimated as $T_{fast} = 1.12 \text{ ns} \pm 0.05 \text{ ns}$ (inset of Fig. 2(b)), close to the values measured for QDs in bulk material, and indicates almost no influence of the cavity mode on the radiative properties of the QD emission due to large spectral mismatch.

The single-photon nature of the collected PL from the QD is verified by measuring the second-order correlation function $g^{(2)}(\tau)$. An auto-correlation measurement was performed on the filtered QD emission under similar excitation conditions close to the saturation power, the result of which is shown in Fig. 2(c). A clear photon antibunching dip is observed at $\tau = 0$ delay with $g^{(2)}(0) = 0.33 \pm 0.04 < 0.5$, indicating the quantum nature of the measured emission line [28]. Having demonstrated the true single-photon generation, the filtered PL was directed to the frequency conversion setup, which was pre-aligned for the optimum conversion efficiency and signal-to-background ratio by using a cw tunable laser at the exact QD emission wavelength, as described before. Figure 2(d) shows the result of an auto-correlation measurement performed on the QD emission line (same excitation conditions as in Fig. 2(c)), now converted to 600nm and directed to a free-space HBT setup as shown in Fig. 1(a). The antibunching dip observed at zero-time delay is measured as $g^{(2)}(0) = 0.24 \pm 0.04 < 0.5$ demonstrating that the converted signal is mainly composed of single-photons, as expected. Due to the narrow bandwidth of the frequency conversion process providing an additional spectral filtering, the antibunching value observed after the conversion is improved.

Similar measurements were carried out under pulsed excitation conditions on device M2. Pulsed measurements provide a convenient way to judge the background levels in the the conversion process, as any noise due to the strong 1550 nm cw beam will uniformly increase the coincidence rates at all times [8], whereas the QD emission is peaked at times corresponding to the repetition period of the excitation laser. They also better represent how such a system might be used in applications for which triggered single photon emission is desirable. The PL spectrum for device M2 is shown in Fig. 3(a), where a bright single QD emission line at 977.04nm is visible next to a cavity mode at 976.65 nm ($Q = 4300$). Figure 3(b) shows the filtered QD emission and the result of time-resolved PL measurement as an inset. The lifetime of the QD emission is estimated as $T_{fast} = 0.93 \text{ ns} \pm 0.05 \text{ ns}$, indicating again almost no in-

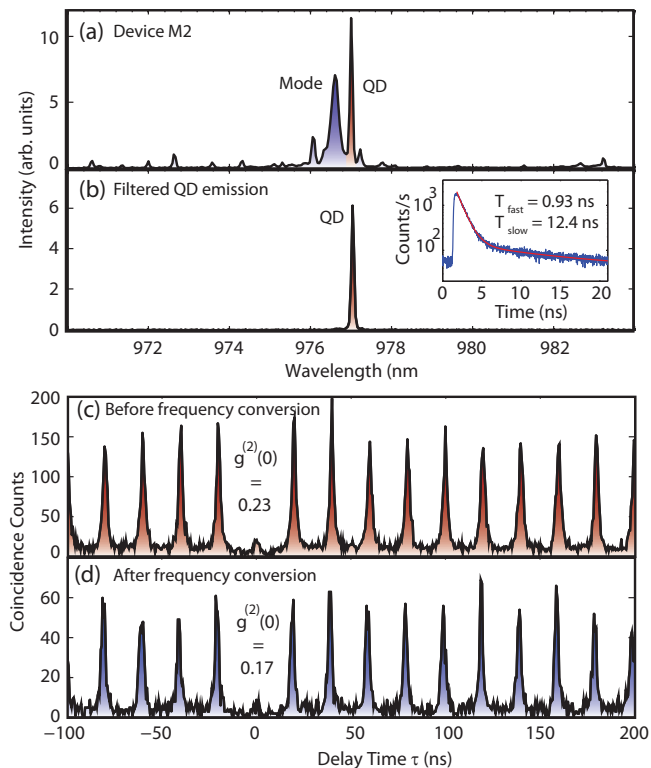


FIG. 3. (a) Low-temperature μ -PL spectrum of device M2 under above-band pulse excitation ($\lambda_{Exc.} = 780$ nm). A bright QD emission and a cavity mode emission with a quality factor $Q = 4300$ are visible around 977 nm. (b) Spectrum of QD emission filtered by a volume Bragg grating. (c)-(d) Second-order autocorrelation function measurements performed on the QD emission line before and after the frequency conversion resulted in $g^{(2)}(0) = 0.23 \pm 0.04$ and $g^{(2)}(0) = 0.17 \pm 0.03$, respectively. inset: Time-resolved PL of the QD emission revealed $T_{fast} = 0.93$ ns \pm 0.05 ns and $T_{slow} = 12.4$ ns \pm 0.1 ns.

fluence of the cavity mode. Before performing frequency conversion, the emission was directed to the HBT setup for photon correlation measurements. A result of such an experiment is shown in Fig. 3(c), where the QD was excited with a pump power close to its saturation. A strong suppression of the peak at zero time delay to a value of $g^{(2)}(0) = 0.23 \pm 0.04 < 0.5$ is observed, thus proving that the filtered PL line is emitted from a single QD [29]. An auto-correlation measurement was then performed on the QD emission after it was converted to 600 nm. As shown in Fig. 3(d), the single-photon nature of the QD emission was preserved during the conversion process, proven by the value of $g^{(2)}(0) = 0.17 \pm 0.03$. The slightly better value of $g^{(2)}(0)$ is a result of the additional filtering provided by the conversion setup. We note that the relatively low coincidence counts observed in Fig. 3(d) are due to the use of a single mode fiber coupled HBT setup for this experiment, where the single mode fiber in-coupling efficiency was 30 %.

In summary, we have demonstrated quantum frequency conversion of single photons emitted from a quantum dot. Photons at 980 nm are converted to 600 nm with a signal-to-background ratio larger than 100 and external conversion efficiency above 40 %. Straightforward engineering of the PPLN waveguide may allow for interfacing commonly-studied 900 nm to 980 nm band quantum dot single photon sources [18–21] with quantum memories near 600 nm, such as in rare-earth doped crystals [30] and neutral atoms [31].

We thank Edward Flagg for information on volume Bragg gratings and Matthew Rakher, Lijun Ma, and Xiao Tang for helpful discussions. S.A. and I.A. acknowledge support under the Cooperative Research Agreement between the University of Maryland and NIST-CNST, Award 70NANB10H193.

* serkan.ates@nist.gov

† kartik.srinivasan@nist.gov

- [1] P. Kumar, *Opt. Lett.* **15**, 1476 (1990).
- [2] M. M. Fejer, G. A. Magel, D. H. Jundt, and R. L. Byer, *IEEE J. Quan. Elec.* **28**, 2631 (1992).
- [3] K. Uesaka, K. Kin-Yip, M.E., Marhic, and L. Kazovsky, *IEEE J. Sel. Top. Quan. Elec.* **8**, 560 (2002).
- [4] A. H. Gnauck, R. Jopson, C. McKinstrie, J. Centanni, and S. Radic, *Opt. Express* **14**, 8989 (2006).
- [5] J. M. Huang and P. Kumar, *Phys. Rev. Lett.* **68**, 2153 (1992).
- [6] Y.-H. Kim, S. P. Kulik, and Y. Shih, *Phys. Rev. Lett.* **86**, 1370 (2001).
- [7] S. Tanzilli, W. Tittel, M. Halder, O. Alibart, P. Baldi, N. Gisin, and H. Zbinden, *Nature* **437**, 116 (2005).
- [8] M. T. Rakher, L. Ma, O. Slattery, X. Tang, and K. Srinivasan, *Nature Photonics* **4**, 786 (2010).
- [9] H. J. McGuinness, M. G. Raymer, C. J. McKinstrie, and S. Radic, *Phys. Rev. Lett.* **105**, 093604 (2010).
- [10] R. Ikuta, Y. Kusaka, T. Kitano, H. Kato, T. Yamamoto, M. Koashi, and N. Imoto, *Nature Communications* **2** (2011).
- [11] S. Zaske, A. Lenhard, C. A. Kessler, J. Kettler, C. Hepp, C. R. Albrecht, W.-M. Schulz, M. Jetter, P. Michler, and C. Becher, <http://www.arxiv.org/abs/1204.6253> (2012).
- [12] A. Vandevender and P. Kwiat, *J. Mod. Opt.* **51**, 1433 (2004).
- [13] C. Langrock, E. Diamanti, R. Roussev, Y. Yamamoto, M. Fejer, and H. Takesue, *Opt. Lett.* **30**, 1725 (2005).
- [14] M. Albota and F. Wong, *Opt. Lett.* **29**, 1449 (2004).
- [15] R. T. Thew, H. Zbinden, and N. Gisin, *Appl. Phys. Lett.* **93**, 071104 (2008).
- [16] L. Ma, O. Slattery, and X. Tang, *Opt. Express* **17**, 14395 (2009).
- [17] C. McKinstrie, J. Harvey, S. Radic, and M. Raymer, *Opt. Express* **13**, 9131 (2005).
- [18] P. Michler, A. Kiraz, C. Becher, W. V. Schoenfeld, P. M. Petroff, L. Zhang, E. Hu, and A. Imamoglu, *Science* **290**, 2282 (2000).
- [19] C. Santori, D. Fattal, J. Vuckovic, G. Solomon, and Y. Yamamoto, *Nature* **419**, 594 (2002).

- [20] E. Moreau, I. Robert, J. Gérard, I. Abram, L. Manin, and V. Thierry-Mieg, *Appl. Phys. Lett.* **79**, 2865 (2001).
- [21] A. J. Shields, *Nature Photonics* **1**, 215 (2007).
- [22] K. Srinivasan and O. Painter, *Nature (London)* **450**, 862 (2007).
- [23] The error bars in (c) are one standard deviation values and are due to fluctuations in the detected count rate on the SPAD.
- [24] M. T. Rakher, L. Ma, M. Davanço, O. Slattery, X. Tang, and K. Srinivasan, *Physical Review Letters* **107**, 083602 (2011).
- [25] J. S. Pelc, L. Ma, C. R. Phillips, Q. Zhang, C. Langrock, O. Slattery, X. Tang, and M. M. Fejer, *Opt. Express* **19**, 21445 (2011).
- [26] H. Dong, H. Pan, Y. Li, E. Wu, and H. Zeng, *Appl. Phys. Lett.* **93**, 071101 (2008).
- [27] Lifetime data is fit to a biexponential function with decay rates T_{fast} and T_{slow} , with the uncertainties given by the fit and representing one standard deviation values.
- [28] $g^{(2)}(\tau)$ under cw excitation is normalized to the coincidence rate at long time delays ($\tau > 500$ ns). The uncertainty in $g^{(2)}(0)$ is due to the fluctuation in coincidence rate for $\tau > 500$ ns, and is the one standard deviation value.
- [29] The $g^{(2)}(0)$ value is determined by comparing the integrated area of the peak around time zero to the average area of the peaks away from time zero. The uncertainty on this value is given by the standard deviation in the area of the peaks away from time zero.
- [30] N. Timoney, B. Lauritzen, I. Usmani, M. Afzelius, and N. Gisin, <http://www.arxiv.org/abs/1202.4314> (2012).
- [31] C. Liu, Z. Dutton, C. H. Behroozi, and L. V. Hau, *Nature* **409**, 490 (2001).